PAPER NAME

**Formulating different RI sensors with gol
d and silver material.pdf**

WORD COUNT	CHARACTER COUNT
9286 Words	**50934 Characters**

PAGE COUNT	FILE SIZE
54 Pages	**1.0MB**

SUBMISSION DATE	REPORT DATE
May 18, 2022 11:47 PM GMT+6	**May 18, 2022 11:50 PM GMT+6**

● **12% Overall Similarity**

The combined total of all matches, including overlapping sources, for each database.

- 8% Internet database
- Crossref database
- 8% Submitted Works database

- 7% Publications database
- Crossref Posted Content database

● **Excluded from Similarity Report**

- Bibliographic material

Declaration of Authorship

We, S.M Towhidul Islam Tonmoy (170021061), Fahmid Mannan (170021060) and Md. Shariful Islam (170021063), declare that this thesis titled, 'Formulating different RI sensors with gold and silver material' and the works presented in it are our own.

We confirm that:

- This work represents partial fulfillment of the requirements for the Bachelor of Science in Electrical and Electronic Engineering degree at Islamic University of Technology.
- No portion of this thesis has been submitted elsewhere for the purpose of earning a degree.
- When we consulted the published work of others, we have always cited our sources explicitly.

Submitted By:

_____

S.M Towhidul Islam Tonmoy (170021061)

_____

Fahmid Mannan (170021060)

_____

Md. Shariful Islam (170021063)

1

Formulating different RI sensors with gold and silver material

Approved By:

20MAY 2022

Prof. Dr. Rakibul Hasan Sagor
Thesis Supervisor,
Professor,
Department of Electrical and Electronic Engineering,
Islamic University of Technology.

2

Formulating different RI sensors with gold and silver material

by

S.M Towhidul Islam Tonmoy (170021061)
Fahmid Mannan (170021060)
Md. Shariful Islam (170021063)

A Thesis Submitted to the Academic Faculty in Partial Fulfillment of the Requirements for the Degree of

BACHELOR OF SCIENCE IN ELECTRICAL AND ELECTRONIC ENGINEERING

Department of Electrical and Electronic Engineering
Islamic University of Technology (IUT)
Gazipur, Bangladesh

May 2022

Declaration of Authorship

We, S.M Towhidul Islam Tonmoy (170021061), Fahmid Mannan (170021060) and Md. Shariful Islam (170021063), declare that this thesis titled, 'Formulating different RI sensors with gold and silver material' and the works presented in it are our own.

We confirm that:

- This work represents partial fulfillment of the requirements for the Bachelor of Science in Electrical and Electronic Engineering degree at Islamic University of Technology.
- No portion of this thesis has been submitted elsewhere for the purpose of earning a degree.
- When we consulted the published work of others, we have always cited our sources explicitly.

Submitted By:

_____

S.M Towhidul Islam Tonmoy (170021061)

_____

Fahmid Mannan (170021060)

_____

Md. Shariful Islam (170021063)

Formulating different RI sensors with gold and silver material

Approved By:

_____

Prof. Dr. Rakibul Hasan Sagor
Thesis Supervisor,
Professor,
Department of Electrical and Electronic Engineering,
Islamic University of Technology.

Abstract

Plasmonic sensors are gaining in popularity as a research topic due to their potential to overcome a number of electronic device flaws. Surface Plasmon Polaritons (SPPs) are a promising choice for producing highly accurate biosensors due to their unique optoelectronic characteristics that exceed the diffraction limit at a nanometer scale. Plasmonic refractive index sensors based on MIM waveguides are gaining popularity for their molecular binding and instant label-free detection. We attempted to develop a plasmonic sensor for the refractive index that had a high degree of sensitivity and optical features that could be tuned. The initial attempted designs along with their performance has been discussed as well. An elaborate physical mechanism of the observed sensor performance i.e. energy streamlines, transmittance spectrum, surface power flow intensity, magnetic and electric field distributions, and sensor performance has been shown here. We also tried to entail how the variation of different parameters has an effect on the performance matrices. Lastly we showcased our future plans and endeavors regarding the design of the plasmonic sensor.

Acknowledgements

First and foremost, we offer gratitude to the Almighty Allah (SWT) for giving us the capability to do this work with good health.

We are grateful to our research supervisor, Rakibul Hasan Sagor, for the support and guidance throughout our research at Islamic University of Technology (IUT). He created a nice research environment for which we were able to explore many ideas without constraint. We have gained a wealth of knowledge and experience in science and engineering through his direction that is beyond value to our future endeavors. For all of his efforts as our true mentor, we express our heartfelt gratitude to him.

We would like to thank our co supervisor Infiter Tathfif Sir and Md. Farhad Hasan sir for their inspiration and help.

And last but not the least we are thankful to our family, friends and well-wishers for their support and inspiration. Without them it would never have been possible for us to make it this far.

Contents

List of figures

Abbreviations

SPP   Surface Plasmon Polariton

SPR   Surface Plasmon Resonance

RI   Refractive Index

FDTD   Finite Difference Time Domain

MIM   Metal Insulator Metal

MDM   Metal Dielectric Metal

FOM   Figure of Merit

FWHM   Full Width Half Maximum

PML   Perfectly Matched Layer

ABC   Absorbing Boundary Condition

TM   Transverse Magnetic

TE   Transverse Electric

POF   Polymer Optical Fibers

CEF   Complex Error Function

B-B   Brendel-Bormann

Chapter 1
Introduction and Background

Attenuated total reflection occurs when photons from an optically condensed medium strikes an optically sparser medium at an inclination larger than the critical angle. As a result, an evanescent wave (EW) originates along the crucial contact. With the aid of TM-polarized input light, free electrons of metals can readily form a surface plasma wave that travels orthogonal to the alloy surface. Surface plasmon resonance is defined as a phenomenon in which the EW and SPW couple and resonate when their frequency, amplitude, and phase are all the same. This makes the reflectivity curve dip at the resonance point. As described in the Kretschmann–Raether (KR) setup, a SPR effect can be developed using a coupling prism. [1,2,4]. The sensitivity of the SPR signal makes it perfect for the detection of different processes. Optical sensors have high sensitivity, low distortion, and strong electrical and chemical reliability. Thus, these signals are frequently used to detect biological changes [5–7] , chemical processes [8–10].

There is a wide variety of biochemical activity that takes place in the sensing medium layer. Some examples of this activity include the detection of human immunoglobulin [11–13], single-stranded DNA or RNA [14–16], and toxic chemical compounds [17–19].

In addition, they are utilized in the monitoring of food safety and the environment. As these RI processes continue to take place, the refractive index of the surrounding environment will shift. Observing these biological or chemical processes may thus be restated by observing changes in the sensor layer's RI. As a result, new research works are seen on SPR biosensors with better sensitivity [20–24] . By assessing changes in light strength, orientation, and other pertinent data, an optical sensor can detect the biological response processes [25, 26].

The refractive index is the most important optical parameter for sensor design.[27]. Real component of the refractive index influences the waveguide phase. On the other hand, the imaginary portion affects lightwave intensity, and asymmetrical distribution determines polarization and chirality.

1.1 Overview of Surface Plasmon Polariton

When metals and dielectric mediums are brought into close proximity with one another, an electromagnetic excitation known as SPP is produced. Additionally, at metallic interfaces, the resonant interaction between SPPs and EM wave radiation produces a remarkably improved spectral near-field.

In the year 1902, Wood made the initial discovery of SPPs when he discovered unexpected characteristics while conducting optical resonance measurements on metallic polarizers [28].

After that, in the year 1908, Mie presented the concept of dispersion by spherical particles [30], and Maxwell Garnett discovered vivid colors in metal-doped glasses [29].

In 1956 [31], Pines illustrated the typical power dissipation experienced by electrons traveling rapidly along metals. He attributed these losses to plasmons, or cohesive vibrations of conduction electrons in the metal [32]. In the corresponding year, Fano came up with the term polariton to describe the vibration of linked electrons and light in a transparent medium.

Ritchie then studied electron energy dissipation in thin films, defining surface plasmons [33]. Using surface plasmon resonances, he explained the unusual activity of metal gratings [34].

After that, Otto and Kretschmann suggested laser-excited metal surface plasmons [35, 36]. Due to its unique properties, SPP-based structures ,data storage devices, solar cells, and sensors, [37] have gained popularity in recent years.

1.2 Literature Review

The index of refraction (RI) is a crucial optical property of materials. Alterations in RI [38] can be utilized to reflect changes in physical specifications, including pressure, concentration, and temperature.

As a consequence of this, RI measurement is applicable in a diverse array of contexts, and it is widely utilized in the fields of diagnosis of diseases [39], food hygiene [41], pollution monitoring [40], and biochemical sensing [42].

Optical fibers detect ocular changes caused by analytes and radiated photons. Optical fiber sensing has progressed since the 1960s. Optical fiber based sensors have distributed sensing, electromagnetic immunity and remote sensing capabilities, unlike electrical sensors [43].

To this day, many different designs of refractive index sensors have been suggested. For instance, the fiber array sensors such as fiber Bragg reflectors [44,45,46], the long-duration fiber reflectors [47,48,49], and the tilted fiber Bragg reflectors [50,51,52] were used for refractive index sensing [53,54,55,56].
In addition to this, for the purpose of RI measurement, two-dimensional materials such as graphene [57,58,59,60] and molybdenum disulfide [61,62,63,64] were incorporated onto the fiber.

The vast majority of published optical fiber refractive index sensors are centered on optical crystal fibers. Despite this, once the structure is altered, the fibers become extremely fragile, rendering them unsuitable for measuring RI in certain scenarios. Polymer optical fibers, in contrast to crystal optical fibers, have the ability to solve problems of this nature.

This particular kind of fiber is made up of polyethylene components that are easy to produce and work with, cheap, very flexible, gentle, and lightweight [65,66]. The high strain limit, ease of operation, and good repeatability of the POF-based sensors make them suitable for use in challenging environments and bending scenarios [67,68]. In addition, polymer materials can be organically doped more easily [69] which provides POF-constructed sensors with promising prospects in the biological discerning domains [70]. POF-based devices have various applications to date, such as temperature detection [71], liquid level detection [72,73], bending measurement [77], displacement detection [74], strain detection [76], PH detection [75], and environment detection [78].

The sensing industry is seeing a rise in the importance of thin metal films, particularly gold, as well as the plasmonic resonance of light that these films possess. Surface Plasmon Resonance, also known as SPR, is one of the approaches that is utilized the majority of the time. This resonant coupling occurs only under

specific optical conditions, such as dielectric and metal permittivity, angle, wavelength, and polarization of the photons impacting the dielectric and metal. Surface-resonant phenomena that are sensitive to optical changes. Alteration in the medium , alters the resonance state and sends a signal. It has been successfully used in applications like enzyme-linked immunosorbent assay (ELISA) which rely on adsorption and desorption of biomolecules [79].

Among them, gold nanoparticles have some interesting properties and are used to keep probes in place and find targets on surfaces requiring sensing with a better detection limit. Like nanoparticles of gold (Au), nanoparticles of silver (Ag) are used in antimicrobial, diagnostic, and therapeutic biotechnology fields [80–83]. It has also been used to make sensor materials, cosmetics, materials that conduct electricity, and parts for electronics. Ag nanoparticles are employed in biosensors to make it easier to detect targets because of their great thermal stability, chemical stability, electrical conductivity, and catalytic activity. Recent research suggests that using Ag nanoparticles in biosensors and bioimaging is both fascinating and effective. The refractive index of most molecules is greater than that of Ag nanoparticles. When a molecule is attached to an Ag nanoparticle, the local refractive index rises, causing the Ag extinction shift to be seen. Different sensors have demonstrated that target molecules may be discovered efficiently using these changes with Ag nanoparticles. Also, putting a protective coating (like silica) atop the silver nanoparticle results in better biomolecular detection [84]. Different chemical and physical methods were used to stabilize Ag nanoparticles, which were then used in different sensors like surface plasmon resonance, Raman spectroscopy, enzyme-linked immunosorbent assay (ELISA), and electrochemical sensors to find different clinical biomarkers with higher sensitivity [85].Reviewing this, the authors talk about how Ag nanoparticles can be used in the biosensor and bioimaging fields.

1.3 Thesis objective:

The thesis aims to design a RI sensor with high sensitivity. Here we have proposed an unique structure with high sensitivity using Ag material employed for bio sensing applications. However, more specifically, the objectives are

- Compare the sensing ranges for gold and silver material for the same structure.

- To obtain validity of the designed sensor by measuring the sensitivity, FOM, Resonant wavelength.
- To summarize important conclusions from the obtained results and discuss the potential applications such as creating datasets with the simulations for using machine learning approaches and checking for bio sensing applications.

1.4 Thesis organization

The thesis has been arranged in the following way-
- In Chapter 2, the basic theory about the propagation of SPP has been described. This chapter introduces the fundamental knowledge and necessary mathematical formulations of SPP propagation at the single and double interface.
- In Chapter 3, the widely used models for modeling metals have been described in detail with necessary derivations. Since SPPs are created by photon energy coupling to metal free electrons, modeling metals is an important step in SPP simulation.
- Since we have developed our simulation model based on the FDTD method, Chapter 4 introduces the fundamentals of the FDTD algorithm for 1D and 2D simulations. The original formulations of Yee do not include the frequency dependent dispersion properties of materials. We have used the ADE based general algorithm for our simulation model which is discussed in Chapter 4. This chapter also discusses the absorbing boundary condition.
- In chapter 5 modified Debye model, Lorentz model is discussed and also a developed simulation model is established.
- In chapter 6 the design of plasmonic sensor along with the Ex,Ey,Ez profiles on the Metal-Dielectric-Metal interfaces will be provided .
- In chapter 7 the validity of the design of the proposed device including the modifications are provided.

Chapter 2
Physics of surface plasmon polaritons

2.1 Fundamentals of Plasmonics

Plasmonics is an emerging field that enables it to confine light in scales shorter than the wavelength beyond the diffraction limit by exploiting the pairing of light to unbound electrons at the exterior of a metal and generating density waves of electrons, called a plasmon. Due to the nature of the plasmon, electrons and photons can coexist on the metal interface under certain conditions to create a new quasiparticle called plasmon polariton [81-82]. Even though the optical properties of plasmons are studied in nanoscale, most of the plasmon's properties are easily developed from the equation of Maxwell without resorting to quantum mechanics since it is the quantization of classical plasma oscillations [83].

2.2 Maxwell's Equations

The four intricate equations that make up Maxwell's equations are essentially the key to unlocking a mathematical understanding of the realm of electromagnetics. Light is a form of electromagnetic radiation, and in an empty space, electromagnetic waves can be modeled using the electric field $\vec{E}$ and magnetic induction $\vec{B}$ $vector$. Maxwell's equations show how these fields interact with matter [84-85], also known as Gauss's Law for electric fields, Gauss's Law for magnetic fields, Faraday's Law, and Ampere's law with Maxwell's addition, are given by:

$$\nabla \cdot \vec{D} = \rho_{ext} \tag{2.1}$$

$$\nabla \cdot \vec{B} = 0 \tag{2.2}$$

$$\nabla \times \vec{E} = -\frac{\partial \vec{B}}{\partial t} \tag{2.3}$$

$$\nabla \times \vec{H} = J_{ext} + \frac{\partial \vec{D}}{\partial t} \tag{2.4}$$

Where,

$\vec{D}$= Electric displacement.

$\vec{B}$= Magnetic induction.

$\vec{E}$= Electric field intensities.

$\vec{H}$= Magnetic field intensities.

ρ_{ext} = Electrons' external charge density.

J_{ext} = External current density.

$\frac{\partial \vec{D}}{\partial t}$ = Displacement current density.

Moreover,

$$\vec{D} = \varepsilon_0 \varepsilon \vec{E} \tag{2.5}$$

$$\vec{B} = \mu_0 \mu \vec{H} \tag{2.6}$$

$$\vec{J} = \sigma \vec{E} \tag{2.7}$$

Where,

ε_0 =Electric permittivity in free space.

μ_0 =Magnetic permeability in free space.

μ = The relative permeability.

σ =Conductivity.

E =Dielectric constant.

2.3 Basic Principles of Localized Surface Plasmon Resonance

When localized electrons in a nanostructure of metal are energized by an adequate incident wavelength, they oscillate and form powerful surface waves [80]. The particle's curved surface exerts an effective restoring force on conduction electrons, allowing resonance. This causes significant field augmentation in the near field zone. This resonance is known as Localized Surface Plasmon Resonance (LSPR). This concept can be theoretically applicable to any metal, as well as alloys with limited imaginary part of electric permittivity and a huge negative real part. Particles interacting with an electromagnetic field, an explicit form of the electromagnetic field distribution can be found using simple assumptions.

To begin, we suppose that the particle size is shorter than the light wavelength in the medium surrounding it. In an electromagnetic field which is oscillating harmonically, the phase is almost unchanged across the volume of the particle. This state can be called quasi-static approximation. Next, a simple geometry is chosen for analysis. A isotropic sphere with homogeneity of radius r_0, a homogenous material surrounding it, non absorbing and isotropic medium. On static electric fields illumination, solving Laplace equation for the potential, $\nabla^2 V = 0$. The solutions for potentials inside and outside of the particle are shown as follows for azimuthal symmetry of the problem and because we require that at the center of the particle the potential will remain finite:

$$V_{in} = -\frac{3\varepsilon_d}{\varepsilon_m(\omega)+2\varepsilon_d}|\vec{E}|r\cos\theta, \; V_{out} = -|\vec{E}|r\cos\theta + \frac{\varepsilon_m(\omega)-\varepsilon_d}{\varepsilon_m(\omega)+2\varepsilon_d}|\vec{E}|r_0^3\frac{\cos\cos\theta}{r^2} \quad (2.8)$$

Where,

$\varepsilon_m(\omega)$ = Electric permittivity of metal.
ε_d = Electric permittivity of the surrounding dielectric layer.
r = Position vector.

$\vec{E}$ = Electric field.

θ = The angle between r and $\vec{E}$.

2.4 Performance Characteristics of Plasmonic Sensors

A discussion is made in this subsection about the main parameters that are used to evaluate the plasmonic RI-sensors. We define the bulk refractive index sensitivity as [86]:

$$S = \frac{dA}{dn} \tag{2.9}$$

Where,
A = Measured parameters (wavelength, angle or intensity).
n = Refractive index of analytes.

In addition, for practical applications we can use the linearity between A and n, so we can consider here a correlation coefficient factor [88].

Another important parameter is figure of merit also known as FOM [89], whose equation can be written as:

$$FOM = \frac{S}{FWHM} \tag{2.10}$$

Here,
FWHM = "Full Width at Half Maximum of resonance spectra".

FOM represents whether the sensors have the ability which can detect the small RI change; thus we require larger FOM values. Due to metals' high intrinsic loss, plasmonic RI sensors have low FOM. We can improve FOM by using optical field coupling. There are also other performance characteristics that are important, such as how accurate the product is, whether or not it is reproducible, and whether or not it has a wide range of applications.The accuracy refers to how closely the value that was measured corresponds to the actual value. Reproducibility refers to the ability of something to produce consistent results while maintaining the same working conditions.

It is important to note that in order to apply plasmonics in practical settings, we will need to strike a balance between the sensors' costs and their levels of performance.

Chapter 3
Dielectric Models for Surface Plasmon Resonance Structure

3.1 Introduction

To generate the absorption coefficient and refractive index values of dielectrics and metals we deploy Dielectric function models at specific wavelengths, and we utilize them to characterize dielectric-metal interface field interactions.

To model optical properties of different materials Drude model is the fundamental and basic one [93–95] and all other models are mainly improved versions of this model. Many scientists experimented to develop new models by directing their focus on primarily experimentally nonparametric models [96, 97] which were not extensive. Widely applied among these are the Brendel-Bormann model [98, 103], Drude-Lorentz model [98–103], and multi oscillator model [104–106] as they were more well founded than other models; although the study of these models are not elaborate in different application situations. Vial et al. [107] explained the scattering characteristics of metals by making use of the Drude Model as opposed to the Drude-Lorentz model. A similar model discussion was presented in a later work [108] by including two crucial points in the Drude-Lorentz model. This was done in order to illustrate the similarities between the two models. The comparison of these models is exciting, but to utilize reliable experimental data as a reference, their validity must be examined.

3.2 Drude model

The Drude model is used to estimate the dispersion characteristics of alloys in the most simple examples of time domain approaches that seek metal-dielectric frequency characterisation. We can estimate a deficient span of wavelength by Drude model [21, 38]:

$$\varepsilon_{Drude}(\omega) = \varepsilon(\infty) - \frac{f_0\omega_p^2}{\omega(\omega-i\Gamma)} \tag{3.1}$$

Here,

f_0 = Oscillator strength.

ω_p = Intraband plasma frequency.

Γ = Scattering frequency.

3.3 Drude-Lorentz model

The Drude-Lorentz model expands the scope of the Drude model's validity as it incorporates the split interband expression [105–107, 109]. The Drude-Lorentz model improves on the Drude model by explicitly separating interband expression. With the addition of this Lorentzian factor, which is defined by a semi-quantum model, the Drude model's range of validity can be expanded significantly[26]. The D-L model is not suitable for explaining abrupt absorption on specific metal edges. According to a number of references, the approximation provided by the Drude-Lorentz model during the beginning of interband absorption does not work well for noble metals like silver, gold, and copper[26]:

$$\varepsilon_{D-L}(\omega) = \varepsilon_{Drude}(\omega) + \sum_{j=1}^{k} \frac{f_j\omega_j^2}{\left(\omega_j^2-\omega^2\right)-i\omega\Gamma_j} \tag{3.2}$$

Here,

ω_j = Oscillator resonant frequencies.

Γ_j = Oscillator resonant bandwidths.

k = Number of oscillators with frequency ω_j.

3.4 Brendel-Bormann model

Brendel-Bormann uses a complex Gaussian error approach in place of the Lorentzian function used by Drude to minimize the errors caused [40]. This avoids the irregular absorption bands that Drude exhibits. Within the Drude model, the performance of Gaussian line shape functions is superior to that of Lorentzian linear shape functions within broadening functions for example, optical characteristics.

In situations where both of these functions have the same full width at half maximum (FWHM) and weight, the wings of the Lorentzian function are typically more stretched out and higher than those of the other function. As a consequence of this, all of the models that are based on Lorentzian show excessive absorption in spite of what is anticipated [98].In order to improve the accuracy of the Drude model, Brendel and Bormann [103] developed a model for the dielectric function of solids that is based on a Gaussian CEF method [40]. A Brendel Bormann polynomial, χ_j is introduced instead of the Lorentzian term in the Drude-Lorentz model, as given in reference [26], which is upgraded by using CEF mechanism [40]. Here k is the number of B-B oscillators. [98, 103].

As a result of such an analytic function, a variable form for the absorption profile may be obtained.:

$$\varepsilon_{B-B}(\omega) = \varepsilon(\infty) - \frac{f_0 \omega_p^2}{\omega(\omega - i\Gamma_0)} + \sum_{j=1}^{k} \chi_j(\omega) \qquad (3.3)$$

Where,
χ_j = BrendelBormann polynomial.

3.5 Multioscillator model

Multioscillator is another interpretation of the Lorentz model that extends the authenticity range by adding different interband concepts [104].
The multiple oscillator model is a widely accepted model for metal dielectric optical characteristics. In the visible spectral ranges, thin metal film wavelength dependencies in optical indices are very complicated [104, 106].

$$\varepsilon_{M-O}(\omega) = \varepsilon(\infty) - \frac{\omega f_0 \omega_p^2 - i f_0 \omega_p^2 \Gamma}{\omega(\omega^2 + \Gamma_0^2)} + \sum_{j=1}^{k} \frac{f_j \omega_{pj}^2 \left(-\omega^2 + \omega_{pj}^2\right) + i\omega f_j \Gamma_j \omega_{pj}^2}{\omega^2 \Gamma_j^2 + \left(-\omega^2 + \omega_{pj}^2\right)^2} \qquad (3.4)$$

Here,

ω_{pj} = Plasmonic resonant frequency.

Γ_j = Oscillator bandwidths.

f_j = Weight factor.

Chapter 4
Overview of Finite-Difference Time-Domain Method

4.1 Introduction to FDTD

Very few methods are as popular as FDTD for the resolution of electromagnetic calculations. It has also been utilized for modeling nano structural devices. The fact that the FDTD approach is incredibly straightforward, even for writing a three-dimensional code, has been one of the key primary attributes. In the early 1970s, K. Yee presented the approach, which was later developed by others.

4.2 1D FDTD

The principle behind the FDTD technique is straightforward. To solve an electromagnetic issue, just discretize in both areas of time and space the Maxwell's equations taking central difference approximations. The novelty of Yee's concept lies in the spatial allocation of the electric and magnetic field portions. We'll start with a basic one-dimensional problem to better comprehend the method's theory. Assume "free space" as a propagation medium at this point. Here, we can write Maxwell's equation as,

$$\frac{\partial E}{\partial t} = \frac{1}{\varepsilon_0} \nabla \times H \qquad (4.1)$$

$$\frac{\partial H}{\partial t} = - \frac{1}{\mu_0} \nabla \times E \tag{4.2}$$

For one-dimensional scenario, we can employ only E_x and H_y and (1), (2) can be rewritten as,

$$\frac{\partial E_x}{\partial t} = - \frac{1}{\varepsilon_0} \frac{\partial H_y}{\partial z} \tag{4.3}$$

$$\frac{\partial H_y}{\partial t} = - \frac{1}{\mu_0} \frac{\partial E_x}{\partial z} \tag{4.4}$$

Here, a plane wave is traveling in the z direction.

Yee's technique considers E_x and H_y shifted by 50% of space in a cell and in time by 50% of a time step while approximating derivatives with central difference.. In such a case, the following equations can be written in this way-

$$\frac{E_x^{n+\frac{1}{2}}(k) - E_x^{n-\frac{1}{2}}(k)}{\Delta t} = - \frac{1}{\varepsilon_0} \frac{H_y^n\left(k+\frac{1}{2}\right) - H_y^n\left(k-\frac{1}{2}\right)}{\Delta z} \tag{4.5}$$

$$\frac{H_y^{n+1}\left(k+\frac{1}{2}\right) - H_y^n\left(k+\frac{1}{2}\right)}{\Delta t} = - \frac{1}{\mu_0} \frac{E_x^{n+\frac{1}{2}}(k+1) - E_x^{n+\frac{1}{2}}(k)}{\Delta z} \tag{4.6}$$

The explicit FDTD equations are obtained from the following

$$E_x^{n+\frac{1}{2}}(k) = E_x^{n-\frac{1}{2}}(k) + \frac{\Delta t}{\varepsilon_0 \Delta z}\left(H_y^n\left(k - \frac{1}{2}\right) - H_y^n\left(k + \frac{1}{2}\right)\right)$$
$$\tag{4.7}$$

$$H_y^{n+1}\left(k + \frac{1}{2}\right) = H_y^n\left(k + \frac{1}{2}\right) + \frac{\Delta t}{\mu_0 \Delta z}\left(E_x^{n+\frac{1}{2}}(k) - E_x^{n+\frac{1}{2}}(k + 1)\right) \tag{4.8}$$

4.3 FDTD in Dielectric

Using Maxwell's equations again we can derive the changes in algorithm. For a generic medium, Maxwell's equations can be written as,

$$E_x^{n+1/2}(k) = \frac{1-\frac{\sigma\Delta t}{2\varepsilon_0\varepsilon_t}}{1+\frac{\sigma\Delta t}{2\varepsilon_0\varepsilon_r}}E_x^{n-1/2}(k) + \frac{\frac{1}{\sqrt{\mu_0\varepsilon_0}}\frac{\Delta t}{\varepsilon_r\Delta z}}{1+\frac{\sigma\Delta t}{2\varepsilon_0\varepsilon_r}}\left(H_y^n(k-1/2) - H_y^n(k+1/2)\right) \quad (4.9)$$

$$H_y^{n+1}\left(k+\frac{1}{2}\right) = H_y^n\left(k+\frac{1}{2}\right) + \frac{1}{\sqrt{\mu_0\varepsilon_0}}\frac{\Delta t}{\Delta z}\left(E_x^{n+\frac{1}{2}}(k) - E_x^{n+\frac{1}{2}}(k+1)\right) \quad (4.10)$$

Chapter 5
Designing Plasmonic Sensor

5.1 Introduction

For plasmonic sensor modeling, the propagation of Surface Plasmon Polariton can be employed. Having developed the simulation model, structures can be such a way that resonant wavelengths vary with reference to alternation of refractive index. For the most accurate realization of the design, appropriate materials must be used. Although, while it is not feasible to create the perfect plasmonic sensor, it may be modeled for extremely excellent performance by adjusting various parameters, which will be addressed in the following sections.

5.2 Initially attempted structures
Hollow Semi- circular arch shaped plasmonic sensor

Structural Parameters of the Proposed RI Nanosensor

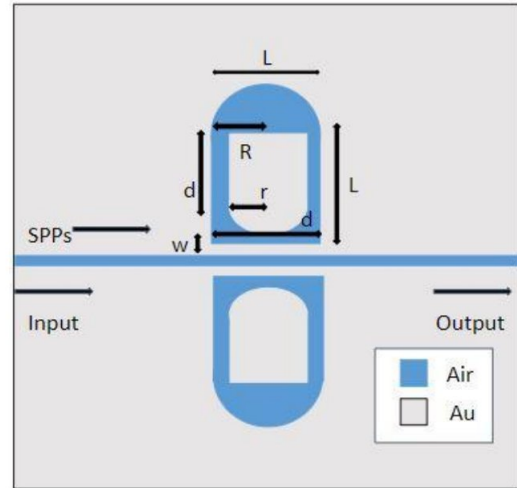| Parameter	Symbol	Value(nm)
Width of the cavity	w	20 nm
Radius of outer semi-circle	R	100 nm
Radius of inner semi-circle	r	80 nm
Length of the outer rectangle	L	200 nm
Height of the outer rectangle	L	200 nm
Length of the inner rectangle	d	160 nm
Length of the inner rectangle	d	160 nm
Gap between cavity and rectangle	w	20 nm

Fig 5.1: Hollow Semi- circular arch shaped plasmonic sensor structure and parameters.
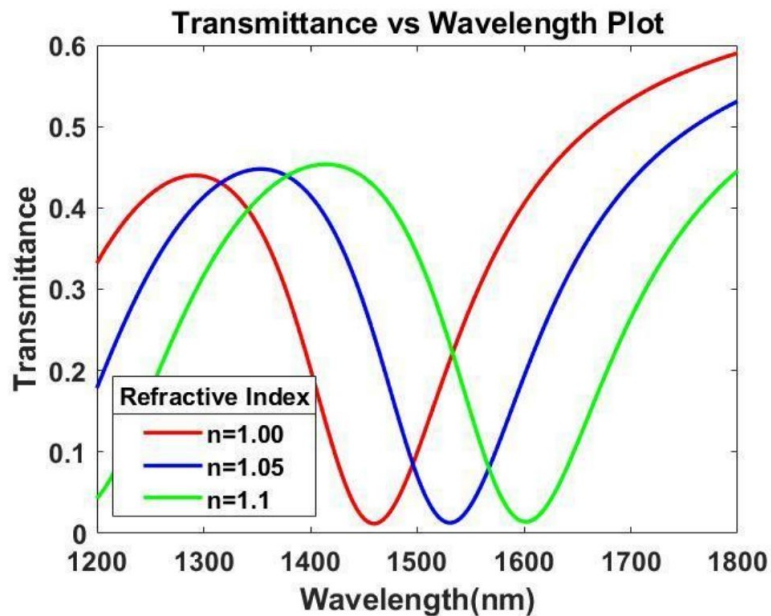

Fig 5.2: Transmittance characteristics of Hollow Semi- circular arch shaped plasmonic sensor.

It has a distinctive capsule form, and the inside chamber was comparable to the exterior covering during the design process. After experimenting with different settings, it was discovered that an arch-shaped inner chamber produces sharper dips and has better sensitivity. The development took place using gold material. The best results have been obtained by shifting the refractive index from 1 to 1.1. By observing the transmittance spectra, we notice that there are Dips obtained at wavelengths 1462 nm, 1532 nm and 1604 nm respectively. The maximum sensitivity obtained was 1440 nm/ RIU.

Butterfly shaped plasmonic sensor

Structural Parameters of the Proposed RI Nanosensor

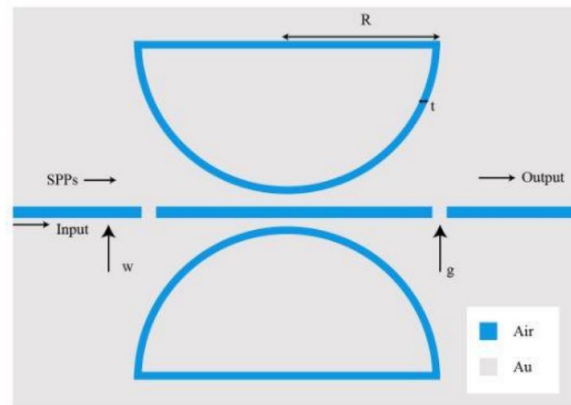| Parameter	Symbol	Value(nm)
Width of the cavity	w	20 nm
Radius of semi-circle	R	300 nm
Thickness between the two semi-circle	t	15 nm
length of the break	g	20 nm

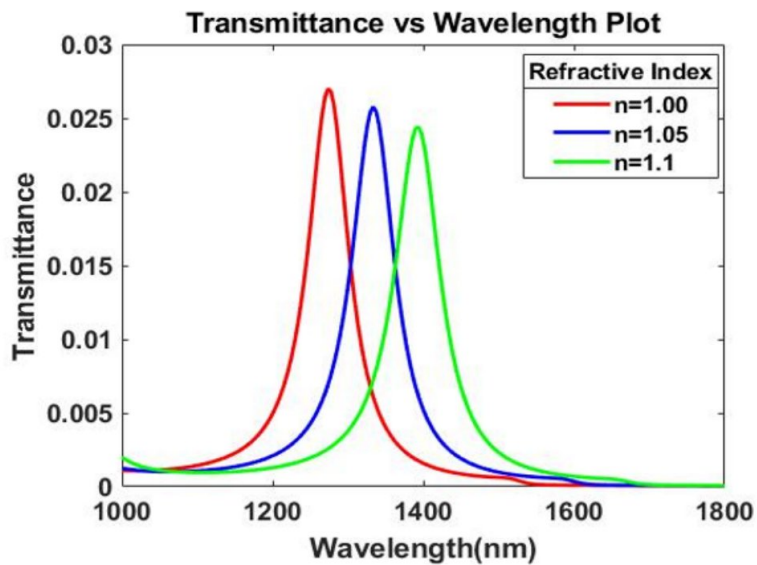Fig 5.3: Butterfly shaped plasmonic sensor structure and parameters.

Fig 5.4: Transmittance characteristics of Butterfly shaped plasmonic sensor.

The first concept was to create two semi-circular rings with horizontal surfaces facing each other. The rings were then flipped vertically, and a butterfly structure was formed. A considerable increase in sensitivity was noted when two breaks were added, and after countless parameter modifications and trial and error the given parameters demonstrated maximum sensitivity. After numerical analysis, it is found that the structures have 3 peaks in 1273nm, 1334nm and 1394 nm respectively and have a sensitivity of 1210nm/RIU.

Magnifying glass shaped plasmonic sensor

Structural Parameters of the Proposed RI Nanosensor

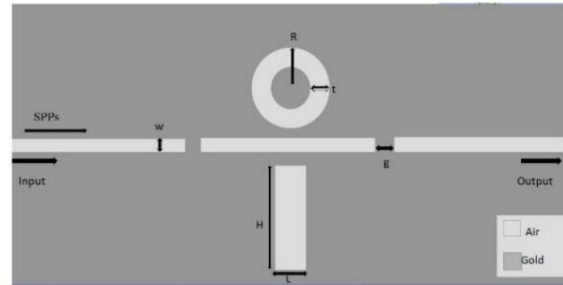| Parameter	Symbol	Value(nm)
Radius of the outer circle	R	125 nm
Thickness of the ring	t	15 nm
Baffle length	g	20 nm
Height of lower groove	h	250 nm
Length of lower groove	l	15 nm
Width of the cavity	w	20 nm

Fig 5.5: Magnifying glass shaped plasmonic sensor structure and parameters.
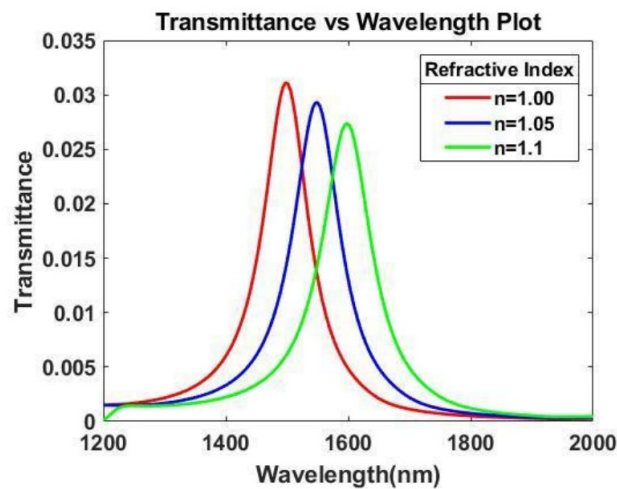

Fig 5.6: Transmittance characteristics of Magnifying glass shaped plasmonic sensor.

As a groove, a ring resonator and a rectangle resonator were employed on either side of the waveguide. Two baffles were placed along the waveguide which resulted in a higher sensitivity. Three peaks were identified at 1497 nm, 1550 nm,

27

and 1598 nm with refractive indexes ranging from 1.0 to 1.1. We estimated the sensitivity using the formula, which is roughly 1010 nm/RIU.

5.3 Final Proposed Sensor Design and Formulation

Fig 5.7: Ring-Type Octagonal Resonator plasmonic sensor structure.

Structural Parameters of the Proposed RI nanosensor

Parameter	Symbol	Value(nm)
Width of the straight waveguide	w	40 nm
Thickness of the octagonal resonator	t	15 nm
Length of outer octagonal side	$L1$	200 nm
Length of inner octagonal side	$L2$	160 nm
Gap between the straight waveguide and the resonator	g	15 nm

The final design of the sensor utilizes an octagonal ring shaped resonator. A linearly straight waveguide has been fitted with the ring-type octagonal resonator. We denote the waveguide width by w, the side length of the octagonal resonator with outer side and inner side of the octagonal shape denoted by L1 and L2 respectively, the thickness of the ring denoted by t, and the gap between the straight waveguide and the resonator symbolized by g are the geometric parameters of the structure of the resonator. The straight waveguide is air filled; the resonator has been filled with the dielectric of which we are going to measure the RI; and the remainder of the design has been filled with silver Ag. The dotted line indicates the input and output ports, which are labeled A and B, respectively. A part of the SPP propagates via the straight waveguide and couples with the resonator before returning to the straight waveguide after completing the effective route. These events cause a wavelength to resonate.

Chapter 6
Performance Analysis of Proposed Plasmonic Sensor

6.1 Performance Analysis

6.1.1 Overview
For Plasmonic Sensors, performance matrices are the sensitivity with respect to the refractive indices and then Figure of Merit (FOM). While the signal is incident on one port, the energy transported by the sensor is measured at both ports one by one. The simulations were carried out for a variety of incident signal wavelengths. We can visualize the performance of the sensor at different wavelengths by plotting the energy measured at the two ports vs. the wavelength of the incident signal.

6.2 Performance Metrics review

Refractive index sensitivity (S) and Figure Of Merit (FOM) are the two key areas focused on to design the proposed plasmonic nanosensors. As stated in chapter 2.3, The sensitivity can be explained as the change of the resonance wavelength, caused due to a change in refractive index.
The Figure Of Merit (FOM) can be calculated with the ratio of sensitivity and the Full Width at Half Maximum (FWHM) value of the resonance spectrum in nm.

6.3 Performance of the Designed Sensor

6.3.1 Electric Field and Transmittance curve
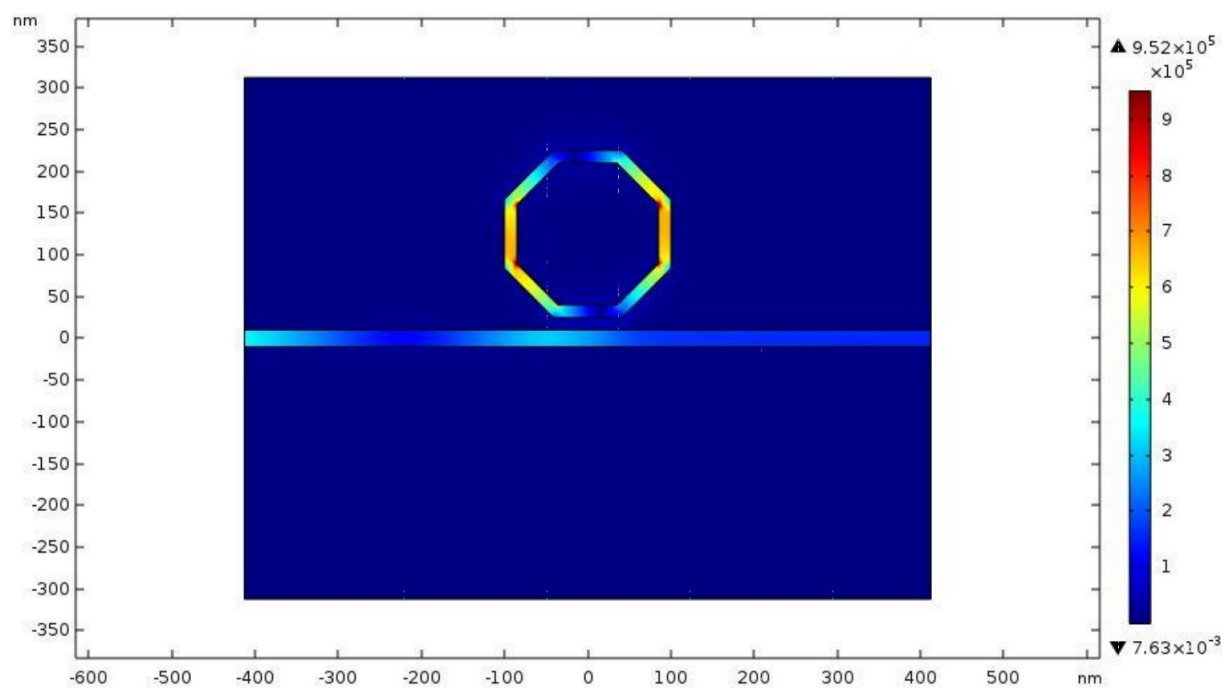
Fig 6.1: Normalized Electric Field of Proposed Sensor.

EM wave normalized electric field components propagating in the design at n = 1 have been presented in the figure.

Fig 6.2: Transmittance vs Wavelength curve.

Using COMSOL Multiphysics,the octagonal resonator transmittance was determined and recorded. The initial simulation was done at a refractive index of value 1, and within the wavelength range of 800 nm to 2000 nm. A dip was obtained at the wavelength 1240 nm.

6.3.2 Sensitivity analysis

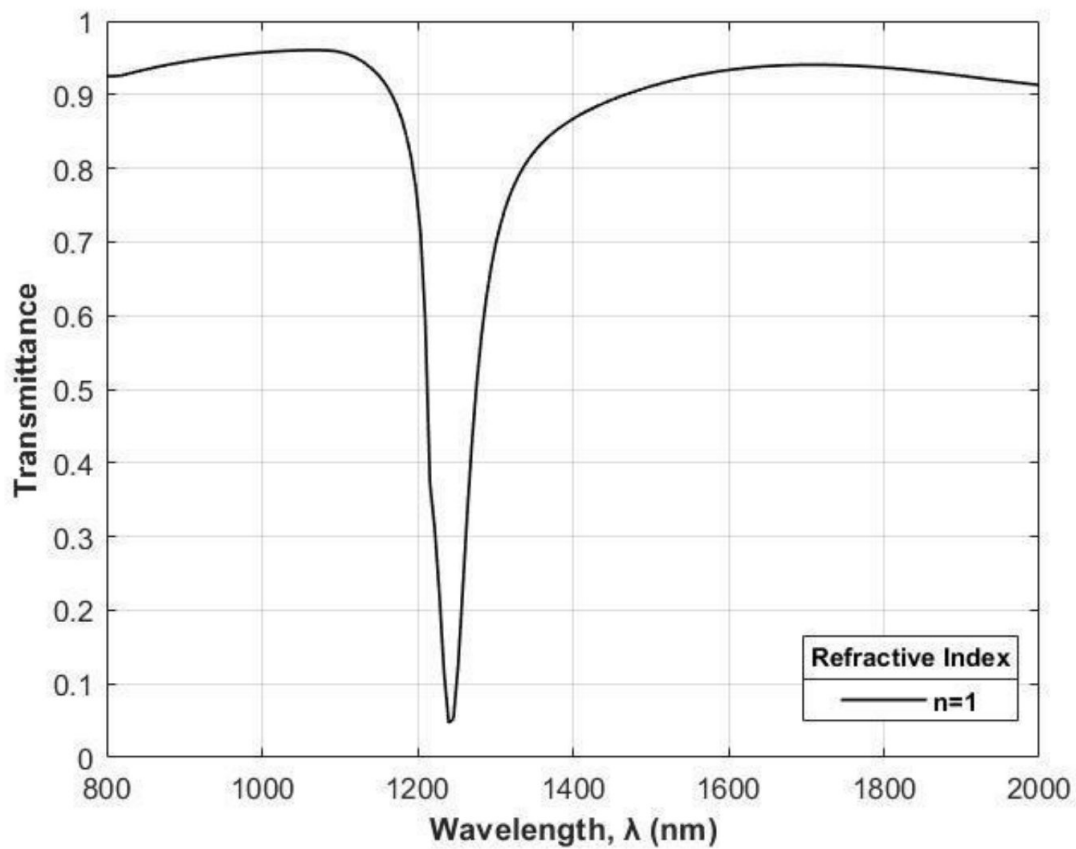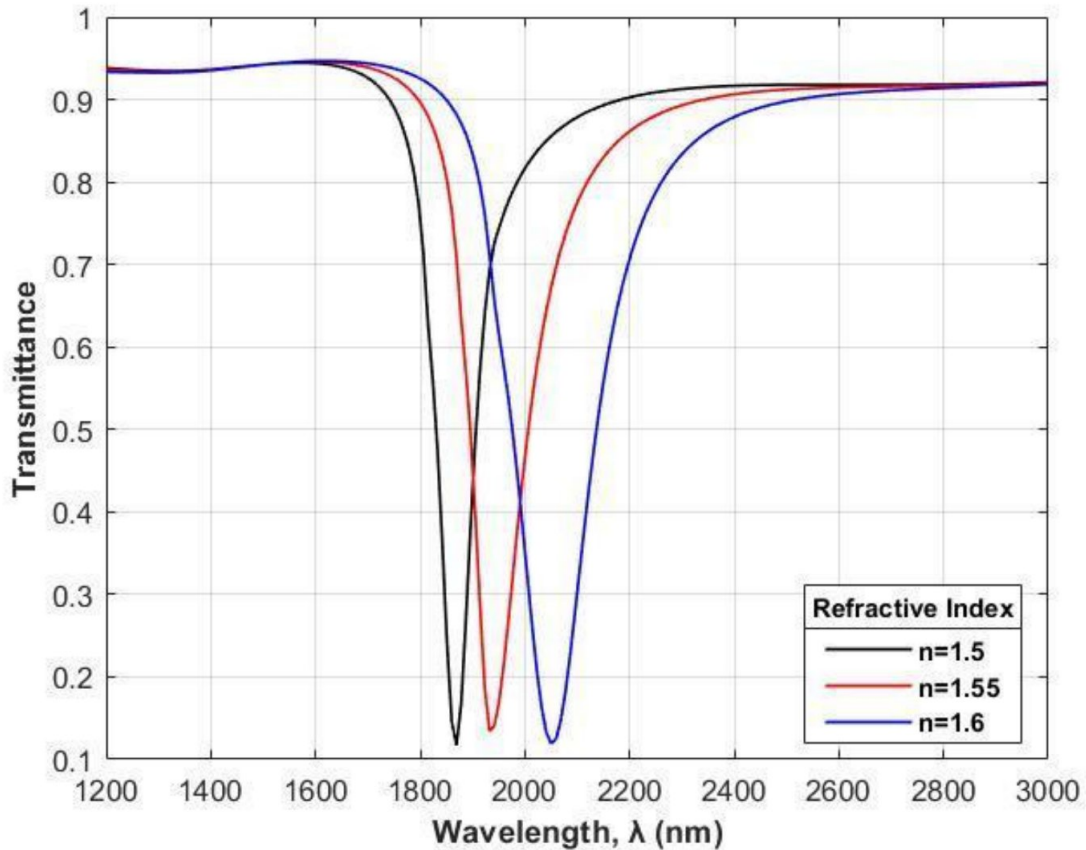Fig 6.3: Transmittance characteristics with respect to varying refractive index of the plasmonic sensor.

To formulate the structure in order to achieve maximum sensitivity, the sensitivity has been calculated for the refractive index variation from n=1.5 to n=1.6 with a step of 0.05. We vary the geometric parameters as the gap, g = 15 nm, Length of outer octagonal side L1 = 200 nm, Length of inner octagonal side L2 = 160 nm, and the thickness of the octagonal ring, t = 15 nm. The maximum sensitivity thus obtained is 2360 nm /RIU and we found its FOM to be 28.3. Further analysis on the variation of the sensitivity depending upon the change of gap between the resonator and the waveguide and thickness of the ring resonator has been carried out in the upcoming sections.

6.3.3 Effect of variation of the gap between resonator and waveguide

(a)   **(b)**
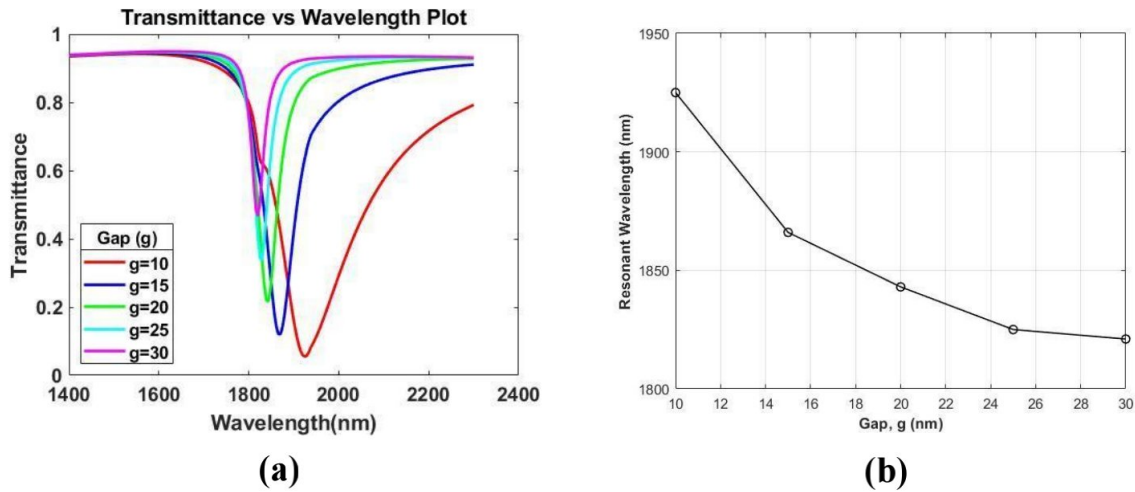
Fig 6.4: Effect of variation of gap in the design of the sensor   (a) Transmittance vs wavelength for different values of gap (b) Resonant wavelength.

Exploring the octagonal structure,we first vary the gap as 10 nm, 15 nm, 20 nm, 25 nm, and 30 nm unchanging the other parameters identical to section 6.3.1 and n=1.5. The simulation demonstrates a blue shift of the transmittance and a gradual declination of resonant wavelength is observed.
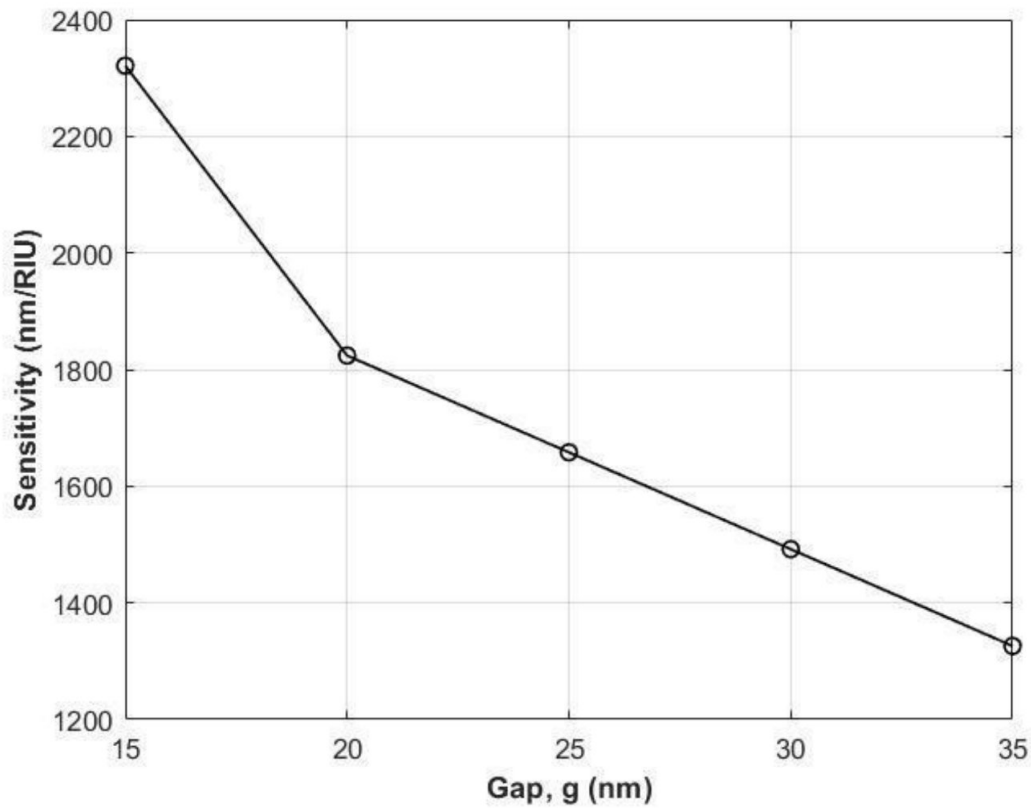
Fig 6.5: Effect of variation of gap in the sensitivity of the designed sensor.

By keeping all the parameters of section 6.3.1 unchanged, the gap between the resonator and waveguide was changed between the values g = 15 to g = 35 with a step of 5. The sensitivity decreases drastically from 2360 nm/RIU to 1824 nm/RIU between the values g = 15 to g = 20 which indicates the requirement of precision of fabrication in this area. From g = 20 to g = 35, a gradual drop of sensitivity occurs from 1824 nm/RIU to 1326 nm/RIU.

35
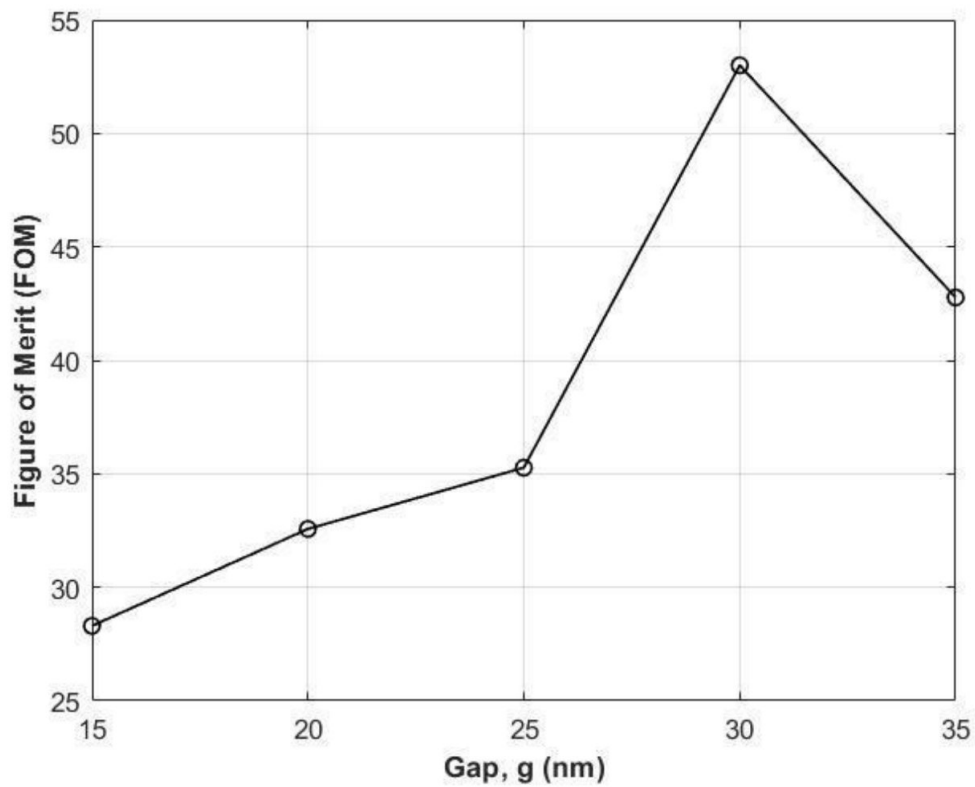
Fig 6.6: Effect of variation of gap in the FOM of the designed sensor.

It was observed that during the shifting of g = 15 to g = 30, the FOM increases, with a dramatic change from 35.27 to 53 in between g values 25 nm to 30 nm. The FOM again begins to drop as g is further increased after 30 nm.

6.3.4 Effect of variation of the thickness of the ring resonator
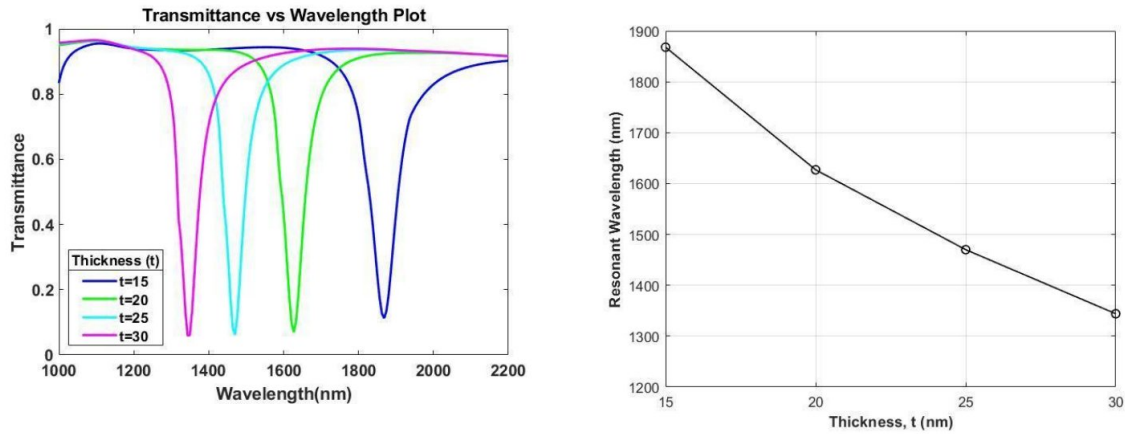
Fig 6.7: Effect of variation of thickness of the ring resonator (a) Transmittance vs wavelength for different values of thickness (b) Resonant wavelength.

To investigate the model, the thickness, t of the ring resonator was varied between 15 nm, 20 nm, 25 nm, and 30 nm while leaving the remaining parameters the same as in section 6.3.1 and n=1.5. This simulation also shows a blue shift in transmittance as well as a gradual declination of the resonant wavelength.
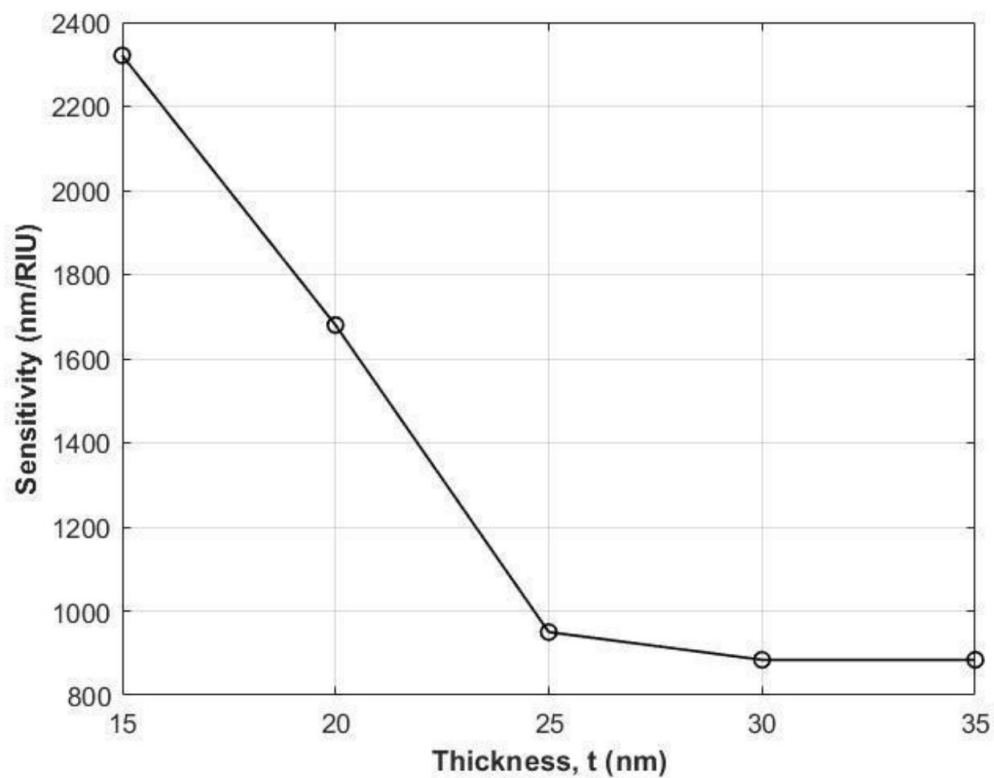
Fig 6.8: Effect of variation of thickness in the sensitivity of the designed sensor.

The thickness of the ring resonator was altered from t = 15 to t = 35 with a step of 5 while keeping all other parameters constant. Between the values g = 15 and g = 25, the sensitivity drops significantly from 2360 nm/RIU to 1680 nm/RIU. The sensitivity is very stable between g = 25 and g = 35.
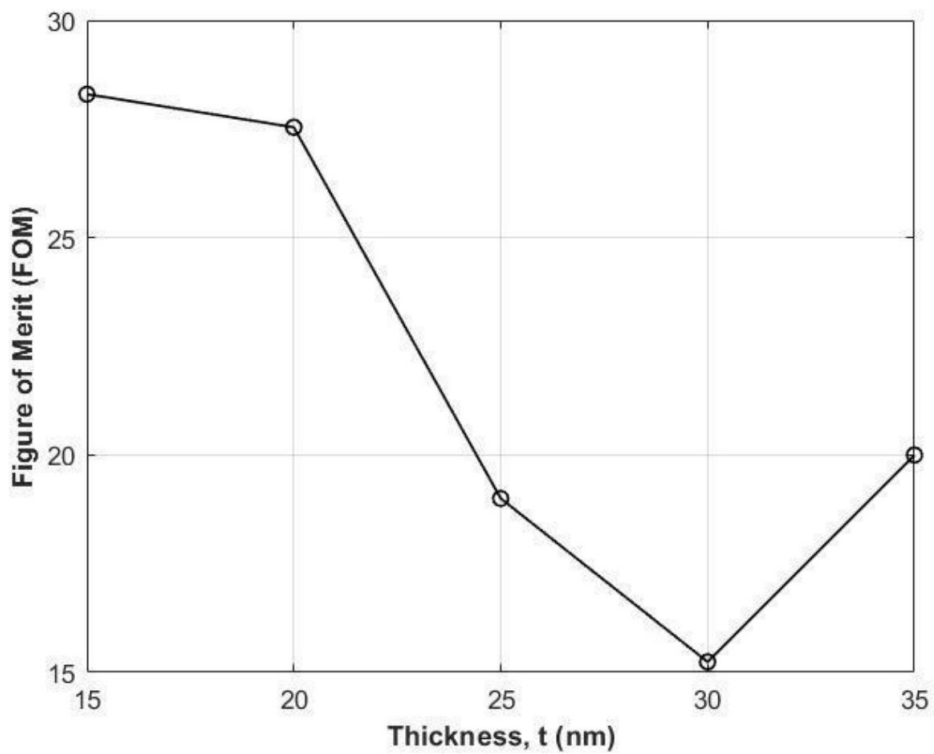
Fig 6.9: Effect of variation of FOM in the sensitivity of the designed sensor.

The FOM essentially remains constant during the transition from g = 15 to g = 20, with a considerable change from 27.54 to 53 between g values 20 nm and 30 nm. After 30 nm, the FOM continues to grow when g increases further.

6.4 Result analysis

From the above discussion we observe a compromise might be required within the performance parameters themselves. For gaps within the value 15-20 we notice a high sensitivity but a drop in the FOM. In this case we prioritize the sensitivity as the primary function of the plasmonic sensor is to sense the change of the analyte with respect to the RI change. FOM is mainly prioritized in the case of formulating plasmonic filters, So we emphasized on the sensitivity and kept the gap of the final design at 15 nm. We also notice that there are sharper dips at higher gaps. This might be because of the variation of energy transmission at the ring resonator because of the change in gap i.e, a lower gap lets in more energy into the ring resonator. We also notice blue shifts on transmittance for increasing the gap and thickness. It is also observed that using silver material instead of gold greatly increases the sensitivity. Finally after careful observations and countless simulations, the structure at section 5.3 is finalized.

Chapter 7
Conclusion and Future works

7.1 Conclusion

We have done about two hundred simulations of different structures. We have planned to store our obtained results and create datasets using those. It will help us to find the pattern of different structures and understand the main reasons behind the variations.

7.2 Future Works

In the future, we plan to use machine learning techniques for plasmonic design. Artificial neural networks enable deep learning methods, which provide a strong and fast tool for constructing precise correlations between plasmonic geometric characteristics and resonance spectra. The spectra of millions of distinct nanostructures may be acquired without the need for expensive simulations, and the cost is merely a one-time expenditure of two thousand groups of training data. This method may be easily extended to other nanophotonic systems of a similar nature, reducing the need for simulation and speeding up the photonic sensor design process.

To give more particular view of the planned future works, following list is provided-

- Improving transmission spectra sensitivity.
- To represent the performance of the frequency converter by spectrum and also find the conversion dependency on composite film dimensions.
- Automatic design of plasmonic nanosensors and reducing the simulation complexities.
- Checking for potential biosensing applications.

References

[1]   Kretschmann, Erwin, and Heinz Raether. "Radiative decay of non radiative surface plasmons excited by light." *Zeitschrift für Naturforschung A* 23.12 : 2135-2136,1968.

[2]   Zayats, Anatoly V., Igor I. Smolyaninov, and Alexei A. Maradudin. "Nano-optics of surface plasmon polaritons." *Physics reports* 408.3-4 : 131-314,2005.

[3]   Pitarke, J. M., et al. "Theory of surface plasmons and surface-plasmon polaritons." *Reports on progress in physics* 70.1 : 1,2006.

[4]   Shalabney, Atef, and Ibrahim Abdulhalim. "Sensitivity‑enhancement methods for surface plasmon sensors." *Laser & Photonics Reviews* 5.4 : 571-606,2011.

[5]   Yuk, Jong Seol, et al. "Sensitivity enhancement of spectral surface plasmon resonance biosensors for the analysis of protein arrays." *European Biophysics Journal* 35.6: 469-476, 2006.

[6]   Xue, Tianyu, et al. "Surface plasmon resonance technique for directly probing the interaction of DNA and graphene oxide and ultra-sensitive biosensing." *Biosensors and Bioelectronics* 58 : 374-379,2014.

[7]   Nanduri, Viswaprakash, et al. "SPR biosensor for the detection of L. monocytogenes using phage-displayed antibody." *Biosensors and Bioelectronics* 23.2 : 248-252,2007.

[8]   Kim, Jang Ah, et al. "Graphene based fiber optic surface plasmon resonance for bio-chemical sensor applications." *Sensors and Actuators B: Chemical* 187 : 426-433,2013.

[9]   Zhao, Yong, Ze-qun Deng, and Jin Li. "Photonic crystal fiber based surface plasmon resonance chemical sensors." *Sensors and Actuators B: Chemical* 202 : 557-567,2014.

[10]   Homola, Jiří. "Present and future of surface plasmon resonance biosensors." *Analytical and bioanalytical chemistry* 377.3 : 528-539,2003.

[11]   Sai, V. V. R., Tapanendu Kundu, and Soumyo Mukherji. "Novel U-bent fiber optic probe for localized surface plasmon resonance based biosensor." *Biosensors and Bioelectronics* 24.9 : 2804-2809,2009.

[12]   Cao, J.; Tu, M.H.; Sun, T.; Grattan, K.T.V. Wavelength-based localized surface plasmon resonance optical fiber biosensor. Sens. Actuators B Chem. 2013, 181, 611–619. [CrossRef]

[13]   Cao, Jie, et al. "Wavelength-based localized surface plasmon resonance optical fiber biosensor." *Sensors and Actuators B: Chemical* 181 : 611-619,2013.

[14]   Xue, Tianyu, et al. "Ultrasensitive detection of miRNA with an antimonene-based surface plasmon resonance sensor." *Nature communications* 10.1 : 1-9, 2019.

[15]   Huang, Xiao, et al. "Graphene‑based electrodes." *Advanced Materials* 24.45: 5979-6004,2012.

[16]   Xue, Tianyu, et al. "A switch of the oxidation state of graphene oxide on a surface plasmon resonance chip." *ACS Applied Materials & Interfaces* 5.6 : 2096-2103,2013.

[17]   Xue, Tianyu, Kun Qi, and Chaoquan Hu. "Novel SPR sensing platform based on superstructure MoS2 nanosheets for ultrasensitive detection of mercury ion." *Sensors and Actuators B: Chemical* 284 : 589-594,2019.

[18]   Zhao, Yuting, et al. "GeSe nanosheets modified surface plasmon resonance sensors for enhancing sensitivity." *Nanophotonics* 9.2 : 327-336,2020.

[19]   Zhu, Jiaqi, et al. "Topological insulator overlayer to enhance the sensitivity and detection limit of surface plasmon resonance sensor." *Nanophotonics* 9.7 : 1941-1951,2020.

[20]   Wang, Jian Jim, et al. "Resonant grating filters as refractive index sensors for chemical and biological detections." *Journal of Vacuum Science & Technology B: Microelectronics and Nanometer Structures Processing, Measurement, and Phenomena* 23.6 : 3006-3010,2005.

43

[21]   Cheng, Yongzhi, et al. "Triple narrow-band plasmonic perfect absorber for refractive index sensing applications of optical frequency." *OSA continuum* 2.7 : 2113-2122, 2019.

[22]   Wu, Tiesheng, et al. "The sensing characteristics of plasmonic waveguide with a ring resonator." *Optics express* 22.7 : 7669-7677, 2014.

[23]   Chen, Tzu-Yin, et al. "Label-free detection of DNA hybridization using transistors based on CVD grown graphene." *Biosensors and Bioelectronics* 41 : 103-109, 2013.

[24]   Chen, Fu, Yongzhi Cheng, and Hui Luo. "Temperature tunable narrow-band terahertz metasurface absorber based on InSb micro-cylinder arrays for enhanced sensing application." *IEEE Access* 8 : 82981-82988,2020.

[25]   Chu, Cheng-Shane, Kun-Zheng Lin, and Yu-Hsuan Tang. "A new optical sensor for sensing oxygen based on phase shift detection." *Sensors and Actuators B: Chemical* 223 : 606-612, 2016.

[26]   York, Timothy, et al. "Bioinspired polarization imaging sensors: from circuits and optics to signal processing algorithms and biomedical applications." *Proceedings of the IEEE* 102.10 : 1450-1469, 2014.

[27]   Liang, Li, et al. "Research progress of terahertz sensor based on artificial microstructure." *Infrared and Laser Engineering* 48.2 : 0203001, 2019.

[28]   Wood, R. W. "XLIV. A suspected case of the electrical resonance of minute metal particles for light-waves. A new type of absorption." *The London, Edinburgh, and Dublin Philosophical Magazine and Journal of Science* 3.16 : 396-410, 1902.

[29]   MAXWELL-GARNETT, J. Cl. "Colors in metal glasses and in metallic films." *Phil. Trans. R. Soc. Lond, A* 203 : 385-420, 1904.

[30]   Fu, Qiang, and Wenbo Sun. "Mie theory for light scattering by a spherical particle in an absorbing medium." *Applied Optics* 40.9 : 1354-1361, 2001.

[31] Pines, David. "Collective energy losses in solids." *Reviews of modern physics* 28.3 : 184, 1956.

[32] Fano, U. "Atomic theory of electromagnetic interactions in dense materials." *Physical Review* 103.5 : 1202, 1956.

[33] Ritchie, Rufus H. "Plasma losses by fast electrons in thin films." *Physical review* 106.5 : 874, 1957.

[34] Ritchie, Rufus H., et al. "Surface-plasmon resonance effect in grating diffraction." *Physical review letters* 21.22 : 1530, 1968.

[35] Otto, Andreas. "Excitation of nonradiative surface plasma waves in silver by the method of frustrated total reflection." *Zeitschrift für Physik A Hadrons and nuclei* 216.4 : 398-410, 1968.

[36] Kretschmann, Erwin, and Heinz Raether. "Radiative decay of non radiative surface plasmons excited by light." *Zeitschrift für Naturforschung A* 23.12 : 2135-2136, 1968.

[37] Barnes, William L., Alain Dereux, and Thomas W. Ebbesen. "Surface plasmon subwavelength optics." *nature* 424.6950 : 824-830, 2003.

[38] Khan, Rana, et al. "Refractive index of biological tissues: Review, measurement techniques, and applications." *Photodiagnosis and Photodynamic Therapy* 33 : 102192, 2021.

[39] Liu, Patricia Yang, et al. "Cell refractive index for cell biology and disease diagnosis: past, present and future." *Lab on a Chip* 16.4 : 634-644, 2016.

[40] Zhang, Ya-nan, et al. "Optical fiber sensors for measurement of heavy metal ion concentration: A review." *Measurement* 158 : 107742, 2020.

[41] Yan, Xu, Hongxia Li, and Xingguang Su. "Review of optical sensors for pesticides." *TrAC Trends in Analytical Chemistry* 103 : 1-20, 2018.

[42] Chen, Yangyang, et al. "Optical biosensors based on refractometric sensing schemes: A review." *Biosensors and Bioelectronics* 144 : 111693, 2019.

45

[43] Lou, Jingyi, Yipei Wang, and Limin Tong. "Microfiber optical sensors: A review." *Sensors* 14.4 : 5823-5844, 2014.

[44] Iadicicco, Agostino, et al. "Thinned fiber Bragg gratings as high sensitivity refractive index sensor." *IEEE Photonics Technology Letters* 16.4 : 1149-1151, 2004.

[45] Tsigaridas, G., et al. "Theoretical and experimental study of refractive index sensors based on etched fiber Bragg gratings." *Sensors and Actuators A: Physical* 209 : 9-15, 2014.

[46] Chryssis, Athanasios N., et al. "High sensitivity evanescent field fiber Bragg grating sensor." *IEEE Photonics Technology Letters* 17.6 : 1253-1255, 2005.

[47] Shen, Fangcheng, et al. "Small-period long-period fiber grating with improved refractive index sensitivity and dual-parameter sensing ability." *Optics Letters* 42.2 : 199-202, 2017.

[48] Shen, Fangcheng, et al. "Compact eccentric long period grating with improved sensitivity in low refractive index region." *Optics Express* 25.14 : 15729-15736, 2017.

[49] Yang, Jianchun, et al. "Sensitivity enhancing of transition mode long-period fiber grating as methane sensor using high refractive index polycarbonate/cryptophane A overlay deposition." *Sensors and Actuators B: Chemical* 207 : 477-480, 2015.

[50] Yan, Zhijun, et al. "Theoretical and experimental analysis of excessively tilted fiber gratings." *Optics express* 24.11 : 12107-12115, 2016.

[51] Jiang, Biqiang, et al. "Temperature-calibrated high-precision refractometer using a tilted fiber Bragg grating." *Optics express* 25.21 : 25910-25918, 2017.

[52] Yan, Zhijun, et al. "All-fiber polarization interference filters based on 45-tilted fiber gratings." *Optics Letters* 37.3 : 353-355, 2012.

[53] Yu, Fangda, Peng Xue, and Jie Zheng. "Enhancement of refractive index sensitivity by bending a core-offset in-line fiber Mach–Zehnder interferometer." *IEEE Sensors Journal* 19.9 : 3328-3334, 2019.

[54] Teng, Chuanxin, et al. "High-sensitivity refractive index sensor based on a cascaded core-offset and macrobending single-mode fiber interferometer." *Frontiers in Materials* : 442, 2021

[55] Zhu, Yongjie, et al. "Refractive index and temperature measurement by cascading macrobending fiber and a sealed alternated SMF-MMF structure." *Optics Communications* 485 : 126738, 2021.

[56] Villatoro, Joel, et al. "Photonic-crystal-fiber-enabled micro-Fabry–Perot interferometer." *Optics letters* 34.16 : 2441-2443, 2009.

[57] Liao, Changrui R., et al. "Fiber in-line Michelson interferometer tip sensor fabricated by femtosecond laser." *IEEE Photonics Technology Letters* 24.22 : 2060-2063, 2012.

[58] Chunyang, Han, et al. "Temperature insensitive refractive index sensor based on single-mode micro-fiber Sagnac loop interferometer." *Applied Physics Letters* 104.18 : 181906, 2014.

[59] Sun, Lipeng, et al. "Miniature highly-birefringent microfiber loop with extremely-high refractive index sensitivity." *Optics express* 20.9 : 10180-10185, 2012.

[60] Sharma, Anuj K., Rajan Jha, and B. D. Gupta. "Fiber-optic sensors based on surface plasmon resonance: a comprehensive review." *IEEE Sensors journal* 7.8 : 1118-1129, 2007.

[61] Liu, Yun, and Wei Peng. "Fiber-optic surface plasmon resonance sensors and biochemical applications: a review." *Journal of Lightwave Technology* 39.12: 3781-3791, 2021

[62] Hu, Xuehao, Patrice Mégret, and Christophe Caucheteur. "Surface plasmon excitation at near-infrared wavelengths in polymer optical fibers." *Optics Letters* 40.17 : 3998-4001, 2015.

[63] Tan, Y. C., et al. "Graphene-deposited photonic crystal fibers for continuous refractive index sensing applications." *Optics Express* 23.24 : 31286-31294, 2015.

[64] Tan, Yang, et al. "Polarization-dependent optical absorption of MoS2 for refractive index sensing." *Scientific reports* 4.1 : 1-6, 2014.

[65] Jin, Yan, and A. M. Granville. "Polymer fiber optic sensors-a mini review of their synthesis and applications." *J. Biosens. Bioelectron* 7.1 : 1-11, 2016.

[67] Bilro, Lúcia, et al. "Optical sensors based on plastic fibers." *Sensors* 12.9 : 12184-12207, 2012.

[68] Soge, Ayodele O., et al. "Recent developments in polymer optical fiber strain sensors: A short review." *Journal of Optics* 50.2 : 299-313, 2021.

[69] Tao, Xiao-ming, Jian-ming Yu, and Hwa-yaw Tam. "Photosensitive polymer optical fibres and gratings." *Transactions of the Institute of Measurement and Control* 29.3-4 : 255-270, 2007.

[70] Cennamo, Nunzio, Maria Pesavento, and Luigi Zeni. "A review on simple and highly sensitive plastic optical fiber probes for bio-chemical sensing." *Sensors and Actuators B: Chemical* 331 : 129393, 2021.

48

[71] Tapetado, A., et al. "Polymer optical fiber temperature sensor with dual-wavelength compensation of power fluctuations." *Journal of Lightwave Technology* 33.13 : 2716-2723, 2015.

[72] Teng, Chuanxin, et al. "Liquid level sensor based on a V-Groove structure plastic optical fiber." *Sensors* 18.9 : 3111, 2018.

[73] Jing, Ning, et al. "A liquid level sensor based on a race-track helical plastic optical fiber." *IEEE Photonics Technology Letters* 29.1 : 158-160, 2016.

[74] Teng, Chuanxin, et al. "Investigation of a plastic optical fiber imprinted with V-groove structure for displacement sensing." *Optical Engineering* 58.7 : 072002, 2019.

[75] Fabbri, Paola, et al. "Poly (ethylene oxide)–silica hybrids entrapping sensitive dyes for biomedical optical pH sensors: Molecular dynamics and optical response." *Optical Materials* 33.8 : 1362-1369, 2011.

[76] Durana, Gaizka, et al. "Use of a novel fiber optical strain sensor for monitoring the vertical deflection of an aircraft flap." *IEEE sensors journal* 9.10 : 1219-1225, 2009.

[77] Leal-Junior, Arnaldo G., et al. "Simultaneous measurement of axial strain, bending and torsion with a single fiber Bragg grating in CYTOP fiber." *Journal of Lightwave Technology* 37.3 : 971-980, 2019.

[78] Min, Rui, et al. "Optical fiber sensing for marine environment and marine structural health monitoring: A review." *Optics & Laser Technology* 140 : 107082, 2021.

[79] Martínez-Hernández, María Elena, et al. "Trends in the implementation of advanced plasmonic materials in optical fiber sensors (2010–2020)." *Chemosensors* 9.4 : 64, 2021.

[80] Liedberg, Bo, Claes Nylander, and Ingemar Lunström. "Surface plasmon resonance for gas detection and biosensing." *Sensors and actuators* 4 : 299-304, 1983.

[81] Dionne, Jennifer A., and Harry A. Atwater. "Plasmonics: metal-worthy methods and materials in nanophotonics." *Mrs Bulletin* 37.8 : 717-724, 2012.

[82] Kholmicheva, Natalia, et al. "Prospects and applications of plasmon-exciton interactions in the near-field regime." *Nanophotonics* 8.4 : 613-628, 2019.

[83] Maier, Stefan A. *Plasmonics: fundamentals and applications*. Vol. 1. New York: springer, 2007.

[84] Khattak, Anum. "Plasmonic Slab Waveguides: Theory & Application for Sensors." ,2020.

[85] Okamoto, Katsunari. *Fundamentals of optical waveguides*. Elsevier, 2021.

[86] Homola, Jiří, Sinclair S. Yee, and Günter Gauglitz. "Surface plasmon resonance sensors." *Sensors and actuators B: Chemical* 54.1-2 : 3-15, 1999.

[87] Degen, Christian L., F. Reinhard, and Paola Cappellaro. "Quantum sensing." *Reviews of modern physics* 89.3 : 035002, 2017.

[88] Gao, Min, et al. "Plasmonic resonance-linewidth shrinkage to boost biosensing." *Photonics Research* 8.7 : 1226-1235, 2020.

[89] Špačková, Barbora, et al. "Optical biosensors based on plasmonic nanostructures: a review." *Proceedings of the IEEE* 104.12 : 2380-2408, 2016.

[90] Homola, Jiří, and Marek Piliarik. "Surface plasmon resonance (SPR) sensors." *Surface plasmon resonance based sensors*. Springer, Berlin, Heidelberg, 45-67, 2006.

[91] Shrivastava, Alankar, and Vipin B. Gupta. "Methods for the determination of limit of detection and limit of quantitation of the analytical methods." *Chronicles of young scientists* 2.1 : 21-25, 2011.

[92] Frascella, Gaetano, et al. "Overcoming detection loss and noise in squeezing-based optical sensing." *npj Quantum Information* 7.1 : 1-6, 2021.

[93] Li, H. Y., et al. "Analysis of the Drude model in metallic films." *Applied optics* 40.34 : 6307-6311, 2001.

[94] Huang, Shuiping, et al. "Determination of optical constants of functional layer of online Low-E glass based on the Drude theory." *Thin solid films* 516.10 : 3179-3183, 2008.

[95] Geraldo, Viviany, et al. "Drude's model calculation rule on electrical transport in Sb-doped SnO2 thin films, deposited via sol–gel." *Journal of Physics and Chemistry of Solids* 67.7 : 1410-1415, 2006.

[96] Amotchkina, Tatiana V., et al. "Comparison of two techniques for reliable characterization of thin metal–dielectric films." *Applied optics* 50.33 : 6189-6197, 2011.

[97] Amotchkina, Tatiana V., et al. "General approach to reliable characterization of thin metal films." *Applied Optics* 50.10 : 1453-1464, 2011

[98] Rakić, Aleksandar D., et al. "Optical properties of metallic films for vertical-cavity optoelectronic devices." *Applied optics* 37.22 : 5271-5283, 1998.

[99] Kadi, Mohamed, Assia Smaali, and Ratiba Outemzabet. "Analysis of optical and related properties of tin oxide thin films determined by Drude-Lorentz model." *Surface and Coatings Technology* 211 : 45-49, 2012.

[100] Smith, G. B., A. I. Maaroof, and A. Gentle. "Homogenized lorentz–drude optical response in highly nanoporous conducting gold layers produced by de-alloying." *Optics Communications* 271.1 : 263-268, 2007.

[101] D'Elia, Stefano, et al. "Ellipsometry investigation of the effects of annealing temperature on the optical properties of indium tin oxide thin films studied by Drude–Lorentz model." *Applied Surface Science* 255.16 : 7203-7211, 2009.

[102] Vázquez-Guardado, A., et al. "Lorentzian-Like Gain in the Analysis of Gain Assisted Slow Surface Plasmon-Polaritons." *Frontiers in Optics*. Optical Society of America, 2012.

[103] Brendel, R., and D. Bormann. "An infrared dielectric function model for amorphous solids." *Journal of applied physics* 71.1 : 1-6, 1992.

[104] Stenzel, O., et al. "The incorporation of metal clusters into thin organic dye layers as a method for producing strongly absorbing composite layers: an oscillator model approach to resonant metal cluster absorption." *Journal of Physics D: Applied Physics* 28.10 : 2154, 1995.

[105] Djurisic, Aleksandra B., Torsten Fritz, and Karl Leo. "Modelling the optical constants of organic thin films: impact of the choice of objective function." *Journal of Optics A: Pure and Applied Optics* 2.5 : 458, 2000.

[106] Sancho-Parramon, Jordi, Vesna Janicki, and Hrvoje Zorc. "Tuning the effective dielectric function of thin film metal-dielectric composites by controlling the deposition temperature." *Journal of Nanophotonics* 5.1 : 051805, 2011.

[107] Vial, Alexandre, and Thierry Laroche. "Description of dispersion properties of metals by means of the critical points model and application to the study of resonant structures using the FDTD method." *Journal of Physics D: Applied Physics* 40.22 : 7152, 2007

[108] Nunes, Frederico Dias, Ben-Hur Viana Borges, and John Weiner. "Analysis of dispersive and dissipative media with optical resonances." *Optics Express* 20.14 : 15679-15691, 2012.

[109] Vial, Alexandre. "Implementation of the critical points model in the recursive convolution method for modelling dispersive media with the finite-difference time domain method." *Journal of Optics A: Pure and Applied Optics* 9.7: 745, 2007.

[110] Palik, Edward D., ed. *Handbook of optical constants of solids*. Vol. 3. Academic press, 1998.

[111] Moon, S. J., et al. "Extended Drude model analysis on multiband Ca2−xSrxRuO4 compounds." *Physica C: Superconductivity and its applications* 460 : 516-517, 2007.

[112] Weideman, J. Andre C. "Computation of the complex error function." *SIAM Journal on Numerical Analysis* 31.5 : 1497-1518, 1994.